CATALYTIC FAST PYROLYSIS OF SOYBEAN HULLS: FOCUS ON THE PRODUCTS

Jose Luis Toro-Trochez[a,b], David Alejandro De Haro Del Río[a], Ladislao Sandoval-Rangel[c], Diana Bustos-Martínez[a], Francisco José García-Mateos[b], Ramiro Ruiz-Rosas[b], José Rodríguez-Mirasol[b], Tomás Cordero[b], Eileen Susana Carrilo-Pedraza[a,*]

[a] Universidad Autónoma de Nuevo León, Facultad de Ciencias Químicas, Ave. Universidad S/N, Cd. Universitaria, San Nicolás de los Garza, N.L., C.P. 66455*, México.*

[b]Universidad de Málaga, Andalucía Tech, Departamento de Ingeniería Química, 29010 Málaga, Spain.

[c] Tecnológico de Monterrey, Escuela de Ingeniería y Ciencias, Ave. Eugenio Garza Sada 2501, Monterrey, N.L., 64849, México.

(*) E-mail: eileen.carrillopd@uanl.edu.mx

Abstract

Catalytic upgrading (with HZSM-5 zeolite) of the fast pyrolysis volatiles obtained from soybean hulls, a low cost and highly available biomass waste, has been investigated. The composition and yield of solid, liquid and non-condensable gas fractions obtained in the 400-600 ºC range during fast pyrolysis (FP) and catalytic fast pyrolysis (CFP) have been compared. The solid, liquid and non-condensable gas fraction obtained during FP and CFP have been characterized and compared. FP of soybean hull delivers liquid yields from 38 to 45 % as temperature increases, while CFP slightly decreases the liquid yield to 37-42 %. The characterization of the bio-oil has revealed that CFP increases more than 21 % the amount of high-value species such as phenols, along with improvements of 30 % in the heating value and reduction of the total acidity number by 15 %. The biogas yield increase in CFP due to the deoxygenation and cracking reactions catalyzed by zeolite HZSM-5. The

composition in FP shifts from being mostly CO_2 and CO at 400 ºC towards a higher presence of hydrogen, methane and C_2-C_3 hydrocarbons at 500-600 ºC. CFP at 500 °C and 600 °C enhances the formation of hydrogen, methane and paraffinic C_2-C_3 hydrocarbons, which boosts the heating value of the gas to more than 15 $kJmol^{-1}$. CFP does not cause any substantial changes in char composition, which is enriched in carbon while losing volatile matter as pyrolysis temperature increases and with char heating values between 25-27 MJ Kg^{-1}. The presence of narrow microporosity has been confirmed by CO_2 physisorption, while SEM images of the char reveal the presence of macropores. These results highlight the benefits of CFP for enhancing the production of bioenergy and bioproducts from soybean hulls.

Keywords (Fast pyrolysis, soybean hulls, biofuel, bio-oil, feedstock, char)

1. Introduction

Fossil fuels satisfies the demand for energy that is required today, with coal, crude oil, and natural gas (account for more than 80% of the world's primary energy) being the main sources of energy [1]. However, concerns about the sustainability of fossil fuels and the environmental problems that derive from their use have prompted the search for new sources of renewable energy.

Renewable energies are mainly used in three sectors: electrical, heat generation, and transportation. In the transport sector, the energy used is produced by ethanol and biodiesel obtained from biomass [2]. Renewable energy represents 11 % and energy from biomass represents 6.9 % of total final energy consumption in the word in 2018 [3], with increasing shares in all sectors, demonstrating the importance of biomass to obtain energy.

One of the most important crops in the world is soybeans with a production in 2020/2021 of 362.1 million metric tons [4] .Within the constituents of soybeans, soybean hulls represents almost 5% (w/w) of production [5], which is equivalent to 17-18 million tons of said residue. The soybean hulls are used as feed of animals or burned in the fields after harvest [6]. The low cost, availability, and abundance of soybean hulls make this feedstock attractive to use for obtaining high-quality liquid fuel or high added-value chemicals [5].

Biomass from agroindustry and forestry wastes, wood, and energy crops is an inexpensive and renewable source, with reduced environmental impacts. It can be transformed through biochemical and thermochemical processes to obtain electrical, thermal, or chemical energy and other products of high value for the chemical industry [7]. Among the thermal processes, pyrolysis stands out because its ability to obtain compounds similar to fossil fuels (oil, coal, biogas), enabling their use as feedstock in current refinery and petrochemical processes. Lignocellulosic biomass pyrolysis is defined as the thermal decomposition of cellulose, hemicellulose, lignin and other minor plant components in the absence of oxygen at

temperatures between 400–800 °C. As a result, bio-oil and non-condensable gases are produced by cooling pyrolytic vapors [8], with a solid residue, charcoal, being obtained as by-product, which could be further processed by gasification to increase the liquid and gas yields [9], or by physical activation to produce activated carbons [10]. The heating rate is an important variable in pyrolysis because it defines the yields and composition of the products. Fast pyrolysis produces greater fragmentation, increasing the volatile yield and by condensation obtain high bio-oil yields than conventional or slow pyrolysis [11]. The latter is used for obtaining char as the main product, with fast pyrolysis being preferred when focusing in the production of bio-oil [12].

Bio-oil is a complex mixture of oxygenates, saturated and unsaturated hydrocarbons, and oxygenated compounds derived from the degradation of the biopolymers present in the biomass. The bio-oil contains a large number of chemical species of high value in other industrial processes such as cyclopentanone used in the pharmaceutical and cosmetic industry [13], furfural and derivates used in chemical, pharmaceutical, agricultural and industrial products [14,15], and phenols used for the production of resins and other value-added compounds [16]. However, the oxygenated compounds present in the bio-oil, such as water, acids, aldehydes, and ketones, are responsible for the drawbacks of the oil for their use or processing into energy products, such as its high viscosity, corrosion, low calorific value, instability in storage conditions and prolonged transport. Consequently, it is necessary to reduce the presence of oxygenated compounds. For instance, they can be transformed into useful chemicals such as hydrocarbons, furans, and phenols used in different industries.

In this sense, catalytic cracking can lead to increased production of desirable compounds, such as hydrocarbons, and decreased content of oxygenates, improving oil characteristics such as acidity, viscosity, and calorific value. Among the different catalysts studied are

inorganic salts, metal oxides, and zeolites [17]. Zeolites have already shown outstanding results in catalytic cracking of bio-oil obtained from pyrolysis [18]; pyrolytic vapors react at acid active sites where deoxygenation and decarboxylation of the adsorbed molecules occurs, improving the properties of the bio-oil [4]. More concretely, Paysepar *et al.* [19] reports that HZSM-5 zeolite promotes the deoxygenation of pyrolytic vapors through dehydration, decarboxylation, and decarbonylation reactions obtaining species of low molecular weight and releasing oxygen in the form of CO_2, CO, and H_2O.

Recently, several works have studied the deoxygenation of pyrolysis vapors of different biomasses using zeolite as a catalyst. For example, Wang *et al*. [20] reported high deoxygenation values of the pyrolytic vapors from cellulose, hemicellulose and lignin biomass using zeolite HZSM-5. Kelkar *et al.* [21] mentioned that the use of HZSM-5 zeolite improves the deoxygenation of lignin pyrolysis vapors by increasing the CO_2 and CO evolution, also increasing the concentration of aromatic organic species and decreasing oxygenated species in the bio-oil. Similarly, Paysepar [19] related the deoxygenation of pyrolysis vapors as depicted by the increase of CO_2 and CO in the gas phase, with the increase of aromatic species in the bio-oil.

Interestingly, there is a lack on the literature concerning the effect of catalytic fast pyrolysis of soybean hulls with HZSM-5. There are some studies on the non-catalyzed pyrolysis of soybean hulls. In a previous work, Toro-Trochez *et al*. [22] carried out conventional pyrolysis of soybean hulls at 600 °C, obtaining a yield in oil and char of around 37 % and 27 %, respectively. Oliveira *et al.* [23] performed fast pyrolysis of soybean hulls, improving the yield to bio-oil up to 45 %. Bio-oil from soybean hulls showed the presence common species such as acids, ketones, and furans. However, they did not use catalysts to reduce the presence of oxygenated species and improve the bio-oil properties. Differently, Uzun *et al.* [24] and

Santos *et al*. [25] performed catalytic fast pyrolysis of soybean residues, reducing the concentration of acidic species, however, soybean hulls where not used in these works.

This work proposes for the first time to the determine the effect of using HZSM-5 zeolite as a catalyst to improve the bio-oil properties obtained in the fast pyrolysis of soybean hulls. Bearing this goal in mind, a catalytic layer of zeolite is added to the fast pyrolysis reactor to catalyze deoxygenation and cracking reactions of the generated vapors. The effect of the zeolite on the product distribution and composition is reported through the detailed characterization of the solid, liquid and non-condensable gas fractions, including the evaluation of their energy contents. As a result, the sustainability of the catalytic fast pyrolysis process using soybean hulls as an alternative and renewable feedstock can be addressed.

2. Experimental

2.1 Material

Soybean hulls (SH) currently listed as agro-industrial waste were obtained from an oil industry in northern Mexico. Biomass residues were grounded and sieved to a particle size between 0.5-0.4mm. The sieved samples were dried at 105 °C in an air-dry oven for 12 h to remove moisture and then stored in closed bottles for later use. SH had already been used in previous works, reporting a composition by weight of 18.5 ± 0.3% hemicellulose, 52.3 ± 0.5 % cellulose, and 3.7 ± 0.4 % lignin [22]. The ultimate analysis of SH revealed a 82.2 ± 0.6 % of volatile material (MV), 2.5 ± 0.1% in inorganic matter (ash), 14.3 ± 0.4 % of fixed carbon and 6.8 ± 0.3 % of moisture

2.2 Catalyst characterization

Zeolite HZSM-5 was obtained from zeolite International (CBV 2314). The zeolite was activated by calcination in air at 600 °C, for 4 hours. The calcined zeolite was analyzed by Fourier transform infrared spectroscopy (FTIR) in a Perkin Elmer Frontier Instrument, equipped with an attenuated total reflectance (ATR) accessory. The spectra were recorded from 4000 to 400 cm^{-1} with 64 scans and a resolution of 0.5 cm^{-1}. To identify the crystalline phase of the calcined zeolites at different temperatures, a D2-Phaser (Bruker) X-ray diffraction kit (XRD) with Cu Kα radiation (λ = 1.5406 Å) was operated at 35 kV and 25 mA, using a 2θ range of 2-50° with a step time of 1 second. The elemental composition of the zeolite and char surface was determined by X-ray fluorescence (XRF), using a PANALYTICAL kit, model EPSILON 3. The porosity of the solids were obtained by nitrogen physisorption at -196 °C and CO_2 at 0 °C, adsorption using a ASAP 2020 equipment (Micromeritics). Before measurement, the samples were degassed for 12 hours at 200 °C in a vacuum. From the N_2 adsorption isotherm, the specific surface area $\left(S_{BET}^{N_2}\right)$ was determined by the Brunauer Emmet and Teller (BET), the micropore volume $\left(V_{DR}^{N_2}\right)$ was

obtained by using the Dubinin-Radushkevich equation, the mesopore volume was determined as the difference between the adsorbed volume of N_2 (P/P_o=0.95) and the micropore volume. From the CO_2 adsorption data, surface area ($S_{DR}^{CO_2}$) and the narrow micropore volume ($V_{DR}^{CO_2}$) were calculated using the Dubinin-Radushkevich. The characterization of coke deposited on the wasted catalysts was carried out by Raman spectroscopy, using an Invia Qontor Raman Confocal Microscope (RENISHAW), using two excitation beams: 514 nm and 785 nm wavelength, and subtracting the fluorescence caused by coke.

2.3 Fast pyrolysis experiments

For the fast pyrolysis (FP) and catalytic fast pyrolysis (CFP) experiments, 5 grams of soybean hulls were used; the sample was placed in a dropper that was connected to the reactor through a ball valve. Once loaded with sample, the dropper was purged using nitrogen. The sample was released into the hot reactor (SS316L, inner diameter: ½", length of the isothermal regime zone: 4 cm) by opening the ball valve. A porous quartz layer at the bottom of the isothermal zone acted as sample holder, retaining the solid product while allowing the volatiles and gases to diffuse towards the reactor outlet. Pyrolysis temperatures were set to 400 °C, 500 °C and 600 °C, and they were tracked by means of a thermocouple placed on top of the quartz layer. A condenser system equipped with a chiller working at -20 ºC was attached to the reactor outlet. For the CFP experiments, a layer of 0.5 g of calcined zeolite at 600 ºC was placed on top of the quartz wool support inside the reactor. A second quartz wool layer was located on top of the catalyst to avoid that the char is mixed with the catalyst during the recovery of the sample (**see fig. S1**). The pyrolysis run was ended after 10 minutes. At that point, the oil obtained from the condensation of the vapors was diluted with ethanol (HPLC grade, signa brand Aldrich USA) and characterized by mass coupled gas chromatography (GC-MS), with an Agilent 6890 series, coupled to an Agilent

5973 Network Mass Selective Detector. The column used was an HP5-MS (Agilent) in a m/z range of 30-550 and helium was used as the eluting gas. The Total Acid number (TAN) value of the bio-oil was calculated following the recommendations on ASTM 664.

The analysis of the non-condensable gases of the FP and CFP at different temperatures (400 °C, 500 °C, and 600°C) was performed by tracking the gases exiting the condenser system. The evolution of CO, CO_2, CH_4 and H_2 was continuously analyzed in a Siemens Ultramat 23 and Calomat systems. Light hydrocarbons (i.e. ethane, ethene, propane, and propane) were collected at the outlet of the condenser using a Tedlar gas sampling bag and quantitatively determined in a Perkin Elmer Autosystem gas chromatograph (GC) equipped with a Hayesep Q (80/100) column and a FID detector. The high heating value (HHV) of the bio-oil samples was obtained using an isoperibolic calorimeter (Parr, model 6200). Approximately 0.2 g of sample was manually introduced inside a calorimetric bomb (Parr, model 1108). Each measurement was repeated at least three times. The HHV of the gas was calculated based as the sum of the HHV of the individual gas components by their molar composition.

2.4 Biomass and char characterization

For the thermogravimetric analysis (TGA) experiment, 10 mg of sample was loaded into the platinum pan, then heated from ambient temperature to 900 °C under dynamic conditions with a heating rate of 5, 10, 30 °C min^{-1}. The carrier gas of the test was nitrogen with a flow rate of 60 mL min^{-1}. The TGA was analyzed with a thermogravimetric analyzer (Q500, TA Instruments, USA). The same equipment was employed for determining the proximate analysis of soybean hulls and char, which was done according to the standard ASTM D3172-07a [26]. The morphology of the char was studied by scanning electron microscopy (SEM) using a Jeol JSM-840 microscope working at 20 kV voltage. The elemental analysis was conducted in a TruSpec micro CHNSO (Leco) analyzer to determine the mass fractions of

carbon (C), hydrogen (H), nitrogen, sulfur and oxygen (O, estimated by difference). The higher heating values calorific values were calculated by Dulong formula [27]:

$$Q_{GCV} = 33.83C + 144.3\left(H - \frac{O}{8}\right) \quad (MJkg^{-1}) \tag{1}$$

3. Results and discussion

3.1 Characterization of zeolite HZSM-5

The characteristic bands of the zeolite HZSM-5 in the range of 400 cm^{-1}-1200 cm^{-1} are showed in **Fig. S2**; the bands in 450 cm^{-1} and 550 cm^{-1} are characteristic of the crystallinity in ZSM zeolites [28]. The band at 450 cm^{-1} was due to the reflection vibration of the AlO_4^{-5} and SiO_4^{-4} tetrahedra, while the band close to 793 cm^{-1} was attributed to the symmetric stretching of the Si-O. A wide band at 1100 cm^{-1} was observed due to the symmetric stretching of Si-O-T (where T can be either Si or Al) [29]. The bands at 560 cm^{-1} and 1232 cm^{-1} were attributed to symmetric and asymmetric stretch vibration, respectively, of the double ring tetrahedrons of the HZSM-5 zeolite; these bands are characteristic of the HZSM-5 zeolite [28].

The DRX at different calcination temperatures of the HZSM-5 zeolite was illustrated in the **Fig. 1** In the XRD patterns at different temperatures the characteristic peaks of the orthorhombic structure of the HZSM-5 zeolite were observed, a doublet at 2θ = 7.9 ° and 8.8° (planes [011] and [200]) , a triplet at 2θ = 23.0°, 23.7° and 24.0° (planes[051], [033] and [313]), the characteristic peaks correspond to JCPDS 44-0003) [30,31]. This analysis confirmed the identity of the zeolite used (HZSM-5) and when working at temperatures below or equal 600 °C the zeolite maintains the crystallinity in its structure. Therefore, the structure does not collapse and can be used for thermal processes, such as fast pyrolysis, when working at a temperature of around 600 °C.

Fig. 1. XRD of the HZSM-5 zeolite at different calcination temperatures

The Si/Al (w/w) ratio was of 42.9 in the zeolite (as revealed by XRF); this can vary between 10 and 140 [32], with the relationship directly affecting the acidic points where ion exchange and different reactions necessary for deoxygenation of pyrolytic vapors occur. A lower Si/Al ratio increases the acidity of the zeolite, and also modifies the particle size and surface area [29]. Future research about CFP of soybean hulls could be focused in using zeolites with different Si/Al ratio.

The N_2 adsorption and desorption isotherm in the HZSM-5 zeolite calcined at 600 °C was reported in **Fig. S3**. In it a point of inflection is observed at low relative pressures and a hysteresis loop, characteristic morphology of type I adsorption isotherms according to the IUPAC classification, typical of microporous solids [33,34]. This behavior is accompanied by a small increase in N_2 adsorbed at medium and high pressures, and a H4 hysteresis loop during desorption that closes at a relative pressure value of 0.45, associated with the presence of narrow slit mesopores. **Table S1** shows the textural characteristics of zeolite HZSM-5. The textural values confirms the prevalent presence of microporosity in this zeolite (micropore volume of 0.16 cc g^{-1}), with a low contribution of mesoporosity. Indeed, the crystalline structure of microporous zeolite HZSM-5 is composed of straight channels (5.3 × 5.6 Å) and zigzag channels (5.1 × 5.5 Å), features which are known to play a relevant role in the catalytic activity and deactivation of zeolites [35]. The textural properties of zeolite have been calculated from the N_2 physisorption measurement. BET surface area close to 450 m^2g^{-1} is obtained, which is in agreement with the values reported by other authors [36].

3.2 Fast pyrolysis and catalytic pyrolysis of soybean hulls

Previous works have demonstrated that SH are a feasible material to use in thermal pyrolysis processes due to the content of volatile matter (VM) of 82 % and low inorganic

content (ash) of 2.6 %, obtaining a high yield of bio-oils and biogas [22]. The high volatile matter in SH is related to the cellulose (52.3 ± 0.5%) and hemicellulose (18.5 ± 0.3%) content, both of them showing high volatilization rates [37], and the lower concentration of lignin (3.7 ± 0.4), i.e. the biopolymer having the largest char yield during pyrolysis. **Fig. 2** shows the weight evolution upon thermal decomposition of SH at three different heating rates. The first derivate of weight (DTG profile, right axis) reveals the presence of a clear peak around 350 ºC (heating rate of 5 ºC min^{-1}, black lines in **Fig. 2**) preceded by a wide shoulder starting at around 240 ºC. These features are shifted to higher temperatures as the heating rate increases (red and blue lines in **Fig. 2**), and they are the result of the simultaneous thermal degradation of three main biopolymeric components [38,39]. The first shoulder can be related to the hemicellulose decomposition, taking place in a temperature range of 200 °C to 315 °C (weight loss of 21 %) [40]. It is followed by the thermal decomposition of cellulose between 315 °C to 415 °C (weight loss of 45 %) [41]. The higher homogeneity and crystallinity of cellulose with respect to hemicellulose explains why the decomposition reaction takes place in a narrower temperature range. Afterwards, the weight loss at temperatures above 415 °C is mainly attributed to decomposition and charring reactions of lignin, which is reported to take part at a wide range of temperature, from 200 to 900 °C [27]. The percentages of thermal degradation of biopolymers vary depending on the rate of heating. As previously mentioned, the experiments conducted at increasing heating rates confirmed that the decomposition reactions shift to higher temperatures with the heating rate. The Kissinger method has been applied to the cellulose decomposition reaction, obtaining an activation energy of only 25.5 kcal mol^{-1} [42]. The low activation energy value is probably the outcome of the thermal lag on the sample [43], with partial control of the reaction by thermal transfer rate, leading to different rates of release of volatile substances along the particle [38]. Consequently, the temperature range for ensure fast and full release of volatiles during fast pyrolysis has been set to 400-600 °C.

Fig. 2. TG (solid lines) and DTG (dotted lines) profiles of SH at different heating rates of 5, 10, 30 °C min^{-1}

The yields of FP and CFP of SH at three different temperatures are compiled in the **Fig. 3**. The lowest yield in bio-oil and the highest yield of char was recorded at 400 °C, attributed to the fact that the biomass had not yet completely volatilized. An increase in temperature promotes the devolatilization of the material, increasing the performance of non-condensable gases and pyrolytic vapors, which by rapid condensation are collected as bio-oil.

Fig. 3. Product distribution from FP and CFP experiments of the SH at different pyrolysis temperatures

Fig. 3 also shows a decrease in the oil yield obtained by CFP at different temperatures (36.5 %, 39.5 % and 41.7 %) compared to the oil obtained with FP (38.1 %, 43.5 % and 45.1 %) due to cracking and deoxygenation reactions at the active sites, allowing the pyrolysis vapors to break into non-condensable gaseous species [44]. Indeed, the decrease in oil yield comes along with the increase of non-condensable gases for CFP in the whole temperature range. Solid yield also decreased in CFP probably due to the removal of the most reactive oxygenated hydrocarbons by the zeolite, which would otherwise have been deposited through secondary condensation reactions forming oligomers and pyrolytic char.

Apart from the gas, liquid, and solid fractions, some coke is formed in the CFP. This coke is produced by the decomposition, repolymerization and condensation reactions of thermally-unstable oxygenates such as aldehydes, phenols, ketones, and acid [45]. At 400°C, cellulose and hemicellulose produces oxygenated species such as furans [46]. So, the coke formed at 400°C is probably produced from the polymeric derivatives and oligomers

resulting from the polymerization of furan by hydrogenation and transfer of hydrogen that occurs at the active sites of the zeolite [47]. Further increase in the pyrolysis temperature produces higher coke deposition in the zeolites. At 500°C, lignin undergoes thermal decomposition [48], releasing phenolic compounds with high re-polymerization capacity. Therefore, the increase in coke content is possibly attributed to repolymerization on the catalyst of lignin derivatives [45,49]

Fig. 4 shows the Raman spectra in the region from 1800 to 1100 cm^{-1}, recorded on wasted zeolite HZSM-5 after CFP process at 400 °C (Z-400) and 600 °C (Z-600). The band around 1350 cm-1 is attributed to disordered aromatic compounds (D) produced throughout the studied temperature range, while the G band is attributed to ordered or graphitic condensed aromatic structures [50]. At 400 °C, coke is mainly composed by amorphous structures, as depicted by the predominant presence of the D band [51]. With the increase in pyrolysis temperature, the peaks of the G-band shifted from 1575 to 1600 cm-1, which indicates the proliferation of aromatic structures. Figure 4 also shows the ratio of intensities G and D of the Raman spectrum bands (IG/ID). The IG/ID ratio increases from 1.1 to 1.35 with temperature, suggesting an increase in both the particle size of the coke and the presence of organized aromatic structures [52]. The surface area of the wasted zeolite obtained at 600 ºC was analyzed by N_2 adsorption at -196 ºC, revealing the decrease in the surface area from 450 to 230 m2g-1. This strong blockage of porosity is probably explained by the increase in the coke yield and particle size.

Fig. 4. Raman spectra of the coke deposited on the HZSM-5 zeolite used at 400 ° C (Z-400) and 600 ° C (Z-600)

3.3 Chemical Species of soybean hulls pyrolytic oil

Table 1 and Fig.5 summarizes the most abundant species found by GC-MS in the oil obtained from FP and CFP of SH. It can be seen that oxygenated compounds are the most abundant compounds in both FP and CFP oil, an expected result given that pyrolytic oil can have more than 400 oxygenated species [53]. These compounds have been grouped into families attending to their functional groups (ketones, furans, phenols, and carbohydrates), however, other functional groups that are part of the soybean hull pyrolytic bio-oil have been reported, such as acids, alcohols, and hydrocarbons [22]. Also, in the pyrolytic bio-oil other functional groups like Hydroxyacetaldehyde, esters, among others, can be present [23]. The difference between the species reported in this study and other studies, can be attributed to the heating rate, operation conditions, the type of biomass, and the analytical conditions of the method used to study the liquid phase [49].In accordance with the SH composition, which is rich in cellulose and hemicellulose, furans and ketones were the main compounds found in the bio-oil. However, compounds that also have a high value in other processes such as cyclopentanone, furfural and phenol were also found [36]. As was previously mentioned, the chemical species with the highest presence in the bio-oil were furans and ketones, which are attributed to the degradation of holocellulose. C5 oxygenated compounds such as furfural or furfuryl alcohol are obtained from hemicellulose decomposition, while C6 oxygenates such as 2-acetylfuran or 5-methylfurfural arises from cellulose. Another important contributor to the formation of furans is the breakdown of levoglucosan molecules produced during the thermal decomposition of cellulose [23]. The presence of levoglucosan and other carbohydrates is also clear, being the most abundant compounds at 400 °C, **Fig. 5**. Further increase on pyrolysis temperature enhances the thermal decomposition of carbohydrates, explaining the decline on their amount and the generation of additional furans and ketones, **Fig. 5 and Table 1**. As for the phenol group, it is seen that their total concentration increases with temperature. The presence of phenol,

cresols and other phenolic species is attributed to the thermal decomposition of lignin, which degrades in a wide temperature range [54]. The increase of phenols at higher pyrolysis temperature is thus explained by the higher thermal stability of lignin. CFP seems to promote the decomposition of lignin oligomers, increasing the formation of phenols and phenolic species (i.e derived from monomeric lignin units).

Table 1. Main compounds and composition (%) as determined by GC-MS obtained from the FP and CFP of SH

Fig. 5. GC-MS derived distribution of chemical compounds in the bio-oil obtained by FP and CFP at different temperatures

It is now clear that the bio-oil was composed mainly of ketones and other oxygenated species, no matter what pyrolysis temperature is used. For this reason, the use of a catalytic process is necessary to improve its properties [55]. When comparing CFP to FP, a decrease in oil yield down to 8% was observed. However, according to the composition data in **Fig. 5**, ketones in the CFP bio-oil show a decline between 37 % to 49 % with respect to FP, while the group of phenols and phenolic compounds increased more than 46 %. Besides, CFP produces several aromatics and cyclic hydrocarbons accounting up to 9 % of the total GC-MS. **Table 2**, compounds were not detected in FP. This is possible because HZSM-5 zeolite has shown selectivity to the formation of alkenes and aromatic hydrocarbons in bio-oil upgrading [56]. Furthermore, the microporous zeolite HZSM-5 has a 10-membered pore system that has straight (5.3 Å x 5.6 Å) and sinusoidal (5.3 Å x 5.5 Å) channels [53], restricting the formation of molecules with an effective folded size smaller than trimethyl benzene [57], possibly giving rise to species that were not formed during FP, such as phenols and furans with alkyl radicals.

Table 2. Main compounds and composition (%) as determined by GC-MS in the CFP

Besides the compounds reported in **Table 1,** it has been reported that acids are the main family of species in pyrolytic soybean hull oil [23], with acetic acid reaching the highest concentration [22], due to the rupture of the acetyl group of hemicellulose during pyrolysis, which represents more than 10 % by weight of hemicellulose [46]. The total acid number (TAN) analysis explains quantitatively how the temperature and the catalyst affect the family of acids obtained in the bio-oil. **Fig. 6** shows the TAN and the higher heating value (HHV) of the bio-oil obtained at different pyrolysis operating conditions. TAN of the bio-oil produced by FP of SH at 400 °C was the highest, with a value of 37 ± 2 mg KOH g^{-1}, due to the thermal decomposition of hemicellulose, and the release of the acetyl group produces acetic acid [46]. Lower TAN values are obtained by increasing the pyrolysis temperature to 500 °C (22 ± 1 mg KOH g^{-1}) and 600 °C (28 ± 2 mg KOH g^{-1}), as more non-acidic compounds are added to the bio-oil, diluting the acids. Interestingly, TAN of bio-oil obtained in CFP is reduced between 14 and 19% depending on the temperature. A similar result was observed in the catalytic deoxygenation of vapors obtained by pyrolysis of wheat straw [58]. This result is probably related to the promotion of catalytic dehydration reaction by HZSM-5. In fact, acetic acid is cracked by HZSM-5 producing intense coke deposition, and steam reforming operating conditions with excess of steam and temperatures over 600 ºC are needed to regenerate the zeolite and allow continuous operation [59].

Fig. 6. Total acid number (TAN) and the higher heating value (HHV) of the FP and CFP of SH.

The increase observed in the HHV of CFP bio-oils (around 30%) is probably related to the larger number of aromatic compounds such as phenols and hydrocarbons produced by the catalytic activity of the zeolite. As for the higher heating value of the liquids, the highest value is obtained by CFP treatment at 600 ºC, reaching 23.1 MJ kg^{-1}. This value is somehow lower than the bio-oil obtained from cellulose [60], however, it is higher than the reported HHV of the bio-oil from corn cob (22.38 MJ kg^{-1}) [61] or wood (16-19 MJ kg^{-1}) [62]. The differences are possibly attributed to the conditions and nature of the feedstock.

3.4 Composition of the non-condensable gas fraction

The **Fig. 7 and Fig. 8.** Shows the molar composition of FP and CFP gases at different temperatures, respectively. Table S2 compiles the molar composition values for the sake of clearness. It must be highlighted that CO_2 and CO are the species with the highest concentration in the entire temperature range studied, although hydrogen, methane, and light hydrocarbons (C_2H_6, C_2H_4, C_3H_8, and C_3H_6) increases their concentration with pyrolysis temperature.

The composition of pyrolysis biogas at 400 °C was 71.0 % CO_2, followed by 27.4 % CO and very low quantities of CH_4 and C_2-C_3 hydrocarbons. The formation of CO_2 under these conditions is attributed to the decomposition of the carboxyl groups present in hemicellulose [57]. As previously discussed in the TGA analysis, hemicellulose is thermally decomposed by pyrolysis process at temperatures below 400 °C. Even though some more CO_2 could be released during pyrolysis at higher temperatures via secondary cracking reactions of volatiles, it is reasonable to consider that CO_2 concentration should decline as the evolution of other gases increases, as observed in **Fig. 7.**

Fig. 7. Molar composition of the gas of the FP of SH

Differently, the CO concentration profile remains constant in the temperature range studied. CO is formed from the decomposition of the carbonyl groups of cellulose and hemicellulose [63], which decompose into different zones and temperatures. In addition, CO at temperatures above 500 °C can be obtained by the decomposition of the carbonyl and carboxyl alkoxyl groups of the lignin side chains [64]. The evolution of CO at the full range of pyrolysis temperature explains the lack of dependence of CO concentration with temperature. Finally, the concentration of hydrogen, methane and light hydrocarbons (C_2-C_3) increases with the operating temperature. The concentration of hydrogen at 400 °C was very low, since H_2 is only released at higher temperatures during cracking and reforming of longer-chain hydrocarbon species and aliphatic or aromatic structures in volatile vapors through side reactions [65,66]**.** These reactions are also responsible of the formation of paraffinic and olefinic C_2 and C_3 hydrocarbons. As for methane, the concentration increases from 0.8% at 400 ºC up to 10.4% at 600°C. The formation of CH_4 was mainly related to the thermal decomposition of aromatic compounds and the breakdown of methoxy groups (O-CH_3) associated with lignin. The **Fig. 8,** the gases in PFC vary similarly to FP.

Fig. 8. Molar composition of the gases of the CFP of SH

To our knowledge, this is the first report of the composition of pyrolysis gases produced in the FP of SH. For this reason, they are compared with other results with similar lignocellulosic composition. The profiles of the non-condensable gases in the FP of SH were similar to those obtained by **Zhao *et al*.** [67] and **Chang *et al***. [68] for the pyrolysis of cellulose and wheat straw, respectively. In addition, the HHV of the gas obtained from pyrolysis at 650 °C of wheat straw (11.45 kJ/m^3) reported by **Chang *et al***. [68] was only

slightly higher than the HHV reported by this study at 600 °C, **Table 3** with the differences probably being explained by the preferential release of H_2 and CH_4, species having higher calorific value, as pyrolysis temperature increases [69].

Table 3 shows the mass concentration of non-condensable gaseous species in the FP and CFP of soybean hulls at different temperatures. Catalytic fast pyrolysis produced deoxygenation reactions such as dehydration, decarboxylation, and decarbonylation, increasing the content of CO and CO_2 in up to 14 and 30 g per 100 g of SH, respectively. In addition, by breaking down low molecular weight molecules such as alcohols and acids, it can form other species such as CH_4 and C_2-C_3 [64]. This scenario may facilitate the formation of H_2 by secondary reactions, increasing the concentration of H_2 at temperatures higher than 500 ºC. Thus, CFP increased the concentration of H_2, CH_4, C_2 and C_3. In accordance with this finding, a proportional increase in the HHVs of non-condensable gases, is observed, **Table 3**. It can be noted that the presence of higher hydrogen concentration also enables the preferential formation of ethane and propane over ethylene and propylene, **Table 3**.

Table 3. Mass yield and HHV of gases in the FP and CFP of the SH at different temperatures

3.5 Characterization of char

Even though some studies report the physicochemical characterization of the carbon obtained from the pyrolysis of soybean at 500 °C [70], there are no studies related to the pyrolytic carbon obtained in the pyrolysis of soybean hull owing to the physicochemical characteristics of the feedstock (material with high volatility and a low percentage of ash) making it more attractive for bio-oil production. As temperature increases char formed during pyrolysis undergoes devolatilization and cracking reactions, delivering an enhanced

formation of the liquid and gaseous product yields [27]. Consequently, the amount of volatile matter as determined by proximate analysis decreases with temperature, **Table 4**, whereas the fixed carbon and ash content slightly increases.

The elemental composition of the char obtained at different temperatures is also included in **Table 4**, revealing that carbon content increases with temperature, while hydrogen and oxygen decreases. It also revealed the presence of nitrogen (2.2-1.6 % wt.), probably as the result of the present of proteins, with the pyrolysis of their amino acids producing the nitrogen doping of the resulting char. These composition results are close to those reported for the pyrolysis of soybean, which produces char useful for agricultural applications, such as a complement to improve nitrogen fertilizers [70].

The calorific value of the chars obtained at different temperatures are summarized in **Table 4**. The HHV of the char (27.2 MJ kg^{-1}) was 60 % higher and 4% lower than that reported in rice husk [71] (17.0 MJ kg^{-1}) and soybean hull (28.1 MJ kg^{-1}) obtained from conventional or slow pyrolysis at 600 °C [22], respectively. The differences were possibly due to the conditions of the experiments such as temperature, heating rate, and the chemical composition of each feedstock.

Table 4. Elemental, proximal and inorganic material analysis of char obtained at different temperatures

Table 4 also shows the inorganic material of the chars obtained at different temperatures. K and Ca were the elements with the highest concentration, with 7.4% and 4.8%, respectively and traces of metals of Mg, Fe, P (less than 1%). The composition on these elements increases after carbonization since they remain in the solid fraction. It has already been reported that K and Ca can act as a catalyst by increasing the release of CO_2 and CO

from carbon in pyrolysis [72,73]. In addition, K could also promote char gasification reactions for the production of physical activated carbons of high surface area [73].

The development of porosity is another feature sometimes observed in char, which enables environmental applications as adsorbents. Fig. S4 reports the N_2 adsorption isotherms at -196 ºC, whereas **Table 5** shows the textural properties derived from the N_2 and CO_2 adsorption isotherms of the chars obtained at different temperatures. The N_2 adsorption isotherm revealed that these chars have very low nitrogen uptake at low relative pressures, followed by an inflection point at medium-high relative pressures. According to the IUPAC, the shape of the isotherms is similar to the type II isotherm of non-porous or macroporous materials [33]. As for the derived porosity parameters, specific surface area increases with pyrolysis temperature up to 7 $m^2\ g^{-1}$, while pore volume increases from 0.002 to 0.004 $cm^3\ g^{-1}$. The higher micropore volume measured by CO_2 adsorption in all samples, Table 5, points out that all of them have a narrow microporosity, with average pore sizes lower than 0.7 nm, in where N_2 adsorption at -196 ºC is hardly measurable [74]. Therefore, these chars have an incipient pore structure resembling in pore size distribution to those of carbon molecular sieves [75]. In addition, CO_2 physisorption shows similar trends than N_2 physisorption with pyrolysis temperature, with an increase in micropore volume from 0.06 m^3g^{-1} to 0.10 m^3g^{-1}. Pore development with the increase in pyrolysis temperature can be related to the decomposition of adsorbed tars, which polymerize and condense on the surface of the char particle during pyrolysis at low temperatures, blocking or even filling the pores [76]. In any case, the observed surface area and pore volume is low for practical applications. For this reason, if applications based on adsorption processes are envisaged for the char obtained under the reported conditions, a subsequent activation stage with physical or chemical methods is necessary [77].

Table 5. Textural parameters of chares obtain at different temperatures

Fig 9 shows the SEM micrographs of the char obtained at different temperatures. Images taken at low magnification reveals that the char consist of long and thin eroded pieces and fragments of the soybean hull. The size of the char particles is lower than those of soybean hulls due to the shrinkage caused by the devolatilization of the biomass during pyrolysis. Furthermore, char particles shows surface cavities of different and irregular sizes (see red circles in Figure 9a), ideal for symbiotic microorganisms such as bacteria (0.3 to 3 μm), fungi (2 to 80 μm), and protozoa (7 to 30 μm), which indicates a possible utility as a fertilizer. These macropores cannot be directly related to the texture results in Table 5, since N_2 and CO_2 physisorption are related to the presence of micropores (<2nm) and mesopores (2-50 nm). The origin of such macropores can be related to the structure of the starting biomass. Soybean hulls have a three-layer structure consisting of a thick outside layer composed by pectin and waxy compounds, an intermediate layer composed by cellulose fibers, and a thin internal layer richer in hemicellulose [78]. SEM images taken at higher magnification, Figure 9b to d, confirms that, after carbonization, the morphology still resembles the original structure of soybean hulls, with some changes related to the different stability of the biopolymers. At 400 ºC, the inner layer is already degraded, probably as an outcome of the low thermal stability of hemicellulose, while the outer and intermediate fiber layers are more or less preserved. At higher pyrolysis temperatures (Fig. 9c and 9d), the fibers of the intermediate layer are emptied, and hollow fibers with lengths between 50 and 100 μm can be clearly seen after pyrolysis at 600 ºC. At these temperatures, the morphology of the lignin shell cementing the external surface of the fibers of the intermediate layer is barely degraded, unlike cellulose and hemicellulose. Thus, the decomposition of the cellulose in the core of the fibers generates the microtubes, Fig. 9d.

Fig. 9. Scanning electron micrographs of the char obtained from pyrolysis of SH at a) lower magnification of char obtained at 500 ºC, b) 400 °C, c) 500 °C and d) 600 °C.

4. Conclusion

The catalytic upgrading of the products obtained from fast pyrolysis of soybean hulls, a low cost and highly available biomass waste, using zeolite HZSM-5 has been investigated for the first time. Fast pyrolysis and catalytic fast pyrolysis experiments have been carried out at temperatures from 400°C to 600 °C.. Similar liquid yields were obtained from FP and CFP (38 to 45% and 37-42%, respectively). Interestingly, the phenol family of products increased more than 16% after CFP. Additionally, increases of 5 % to 9 % are obtained in the hydrocarbon species, whereas the ketone family decreased around 37-49 %. Consequently, a 14 % to 19 % decrease in the TAN is observed owing to the cracking of acetic and other organic acids. This change in the composition of the bio-oil increased the HHV around 30% after CFP. Gas yield increased in CFP due to the deoxygenation and cracking reaction catalyzed by zeolite HZSM-5. In addition, the biogas and the char can be used to generate energy, showing maximum HHV values of 15.6 MJ mol^{-1} and 24.2 MJ Kg^{-1}, respectively. CFP does not cause any substantial changes in char composition.

These results highlight the benefits of CFP for enhancing the production of bioenergy and bioproducts from soybean hulls. In addition, the characterization of the porosity and morphology of the char obtained as a co-product enables its possible application as adsorbent or fertilizer. Furthermore, considering the results obtained in this studio, additional research could explore the use of new catalysts and improvements in the zeolite to optimize the CFP process and maximize the energy output of the products.

Acknowledgements

The authors wish to thank the Universidad Autónoma de Nuevo León for permit the development of this work and the Tecnológico de Monterrey for allowing the use of its facilities and equipment. The authors also thank the Spanish government and MICINN (RTI2018-097555-B-100) for financial support. The authors also acknowledge to the Universidad de Malaga for allowing the use of its facilities and equipment.

References

[1] W. Wang, L.W. Fan, P. Zhou, Evolution of global fossil fuel trade dependencies, Energy. 238 (2022) 121924. https://doi.org/10.1016/J.ENERGY.2021.121924.

[2] Renewable Energy policy Network for the 21st Century, Energías renovables 2017 reporte de la situación mundial, España, 2017.

[3] A. Thomas, A. Fabiani, B. Adam, F. Guerra, R. Levin, Renewables 2020 Global Status Report, Paris, France, 2020. https://abdn.pure.elsevier.com/en/en/researchoutput/ren21(5d1212f6-d863-45f7-8979-5f68a61e380e).html.

[4] G.A. Bittencourt, L.P. de S. Vandenberghe, K.K. Valladares-Diestra, L.W. Herrmann, A.F.M. de Mello, Z.S. Vásquez, S.G. Karp, C.R. Soccol, Soybean hulls as carbohydrate feedstock for medium to high-value biomolecule production in biorefineries: A review, Bioresour. Technol. 338 (2021) 125594. https://doi.org/10.1016/j.biortech.2021.125594.

[5] G.F. Giri, G. Viarengo, R.L.E. Furlán, A.G. Suárez, E. Garcia Véscovi, R.A. Spanevello, Soybean hulls, an alternative source of bioactive compounds: Combining pyrolysis with bioguided fractionation, Ind. Crops Prod. 105 (2017) 113–123. https://doi.org/10.1016/J.INDCROP.2017.05.005.

[6] Q. Qing, Q. Guo, L. Zhou, X. Gao, X. Lu, Y. Zhang, Comparison of alkaline and acid pretreatments for enzymatic hydrolysis of soybean hull and soybean straw to produce fermentable sugars, Ind. Crops Prod. 109 (2017) 391–397. https://doi.org/10.1016/j.indcrop.2017.08.051.

[7] V. Dhyani, T. Bhaskar, A comprehensive review on the pyrolysis of lignocellulosic biomass, Renew. Energy. 129 (2017) 695–716. https://doi.org/10.1016/j.renene.2017.04.035.

[8] S.D. Stefanidis, K.G. Kalogiannis, E.F. Iliopoulou, A.A. Lappas, P.A. Pilavachi, In-situ upgrading of biomass pyrolysis vapors: Catalyst screening on a fixed bed reactor, Bioresour. Technol. 102 (2011) 8261–8267. https://doi.org/10.1016/j.biortech.2011.06.032.

[9] J. Alvarez, G. Lopez, M. Amutio, J. Bilbao, M. Olazar, Evolution of biomass char features and their role in the reactivity during steam gasification in a conical spouted bed reactor, Energy Convers. Manag. 181 (2019) 214–222. https://doi.org/10.1016/J.ENCONMAN.2018.12.008.

[10] J.M. Rosas, R. Ruiz-Rosas, J. Rodríguez-Mirasol, T. Cordero, Kinetic study of the

oxidation resistance of phosphorus-containing activated carbons, Carbon N. Y. 50 (2012) 1523–1537. https://doi.org/10.1016/j.carbon.2011.11.030.

[11] J. Akhtar, N. Saidina Amin, A review on operating parameters for optimum liquid oil yield in biomass pyrolysis, Renew. Sustain. Energy Rev. 16 (2012) 5101–5109. https://doi.org/10.1016/j.rser.2012.05.033.

[12] J.I. Montoya, F. Chejne-Janna, M. Garcia-Pérez, Fast pyrolysis of biomass: A review of relevant aspects. Part I: Parametric study, Dyna. 82 (2015) 239–248. https://doi.org/10.15446/dyna.v82n192.44701.

[13] M. Hronec, K. Fulajtarová, Selective transformation of furfural to cyclopentanone, Catal. Commun. 24 (2012) 100–104. https://doi.org/10.1016/J.CATCOM.2012.03.020.

[14] H.E. Hoydonckx, W.M. Van Rhijn, W. Van Rhijn, D.E. De Vos, P.A. Jacobs, Furfural and Derivatives, Ullmann's Encycl. Ind. Chem. (2007). https://doi.org/10.1002/14356007.A12_119.PUB2.

[15] R. Mariscal, P. Maireles-Torres, M. Ojeda, I. Sádaba, M.L. Granados, Furfural: a renewable and versatile platform molecule for the synthesis of chemicals and fuels, Energy Environ. Sci. 9 (2016) 1144–1189. https://doi.org/10.1039/C5EE02666K.

[16] A. Effendi, H. Gerhauser, A. V. Bridgwater, Production of renewable phenolic resins by thermochemical conversion of biomass: A review, Renew. Sustain. Energy Rev. 12 (2008) 2092–2116. https://doi.org/10.1016/j.rser.2007.04.008.

[17] Y. Wang, Q. Yang, L. Ke, Y. Peng, Y. Liu, Q. Wu, X. Tian, L. Dai, R. Ruan, L. Jiang, Review on the catalytic pyrolysis of waste oil for the production of renewable hydrocarbon fuels, Fuel. 283 (2021) 119170. https://doi.org/10.1016/J.FUEL.2020.119170.

[18] D. Wang, R. Xiao, H. Zhang, G. He, Journal of Analytical and Applied Pyrolysis Comparison of catalytic pyrolysis of biomass with MCM-41 and CaO catalysts by using TGA – FTIR analysis, J. Anal. Appl. Pyrolysis. 89 (2010) 171–177. https://doi.org/10.1016/j.jaap.2010.07.008.

[19] H. Paysepar, K.T.V. Rao, Z. Yuan, H. Shui, C. (Charles) Xu, Improving activity of ZSM-5 zeolite catalyst for the production of monomeric aromatics/phenolics from hydrolysis lignin via catalytic fast pyrolysis, Appl. Catal. A Gen. 563 (2018) 154–162. https://doi.org/10.1016/j.apcata.2018.07.003.

[20] K. Wang, K.H. Kim, R.C. Brown, Catalytic pyrolysis of individual components of lignocellulosic biomass, Green Chem. 16 (2014) 727–735.

https://doi.org/10.1039/c3gc41288a.

[21] S. Kelkar, C.M. Saffron, K. Andreassi, Z. Li, A. Murkute, D.J. Miller, T.J. Pinnavaia, R.M. Kriegel, Applied Catalysis B : Environmental A survey of catalysts for aromatics from fast pyrolysis of biomass, 175 (2015) 85–95.

[22] J.L. Toro-Trochez, E.S. Carrillo-Pedraza, D. Bustos-Martínez, F.J. García-Mateos, R.R. Ruiz-Rosas, J. Rodríguez-Mirasol, T. Cordero, Thermogravimetric characterization and pyrolysis of soybean hulls, Bioresour. Technol. Reports. 6 (2019) 183–189. https://doi.org/10.1016/J.BITEB.2019.02.009.

[23] T.J.P. Oliveira, C.R. Cardoso, C.H. Ataíde, Fast pyrolysis of soybean hulls: Analysis of bio-oil produced in a fluidized bed reactor and of vapor obtained in analytical pyrolysis, J. Therm. Anal. Calorim. 120 (2015) 427–438. https://doi.org/10.1007/s10973-015-4600-6.

[24] B.B. Uzun, A.E. Pütün, E. Pütün, Fast pyrolysis of soybean cake: Product yields and compositions, Bioresour. Technol. 97 (2006) 569–576. https://doi.org/10.1016/j.biortech.2005.03.026.

[25] A.L.F. Santos, D.U. Martins, O.K. Iha, R.A.M. Ribeiro, R.L. Quirino, P.A.Z. Suarez, Agro-industrial residues as low-price feedstock for diesel-like fuel production by thermal cracking, Bioresour. Technol. 101 (2010) 6157–6162. https://doi.org/10.1016/J.BIORTECH.2010.02.100.

[26] ASTM, D3172-07a Standard Practice for Proximate Analysis of Coal and Coke. ASTM International, West Conshohocken, PA., 2007.

[27] E. Pehlivan, N. Özbay, A.S. Yargiç, R.Z. Şahin, Production and characterization of chars from cherry pulp via pyrolysis, J. Environ. Manage. (2016). https://doi.org/10.1016/j.jenvman.2017.05.002.

[28] G. Coudurier, C. Naccache, J.C. Vedrine, Uses of I.R. Spectroscopy in identifying ZSM Zeolite Structure, (1982) 1413–1415.

[29] L. Shirazi, E. Jamshidi, M.R. Ghasemi, The effect of Si/Al ratio of ZSM-5 zeolite on its morphology, acidity and crystal size, Cryst. Res. Technol. 43 (2008) 1300–1306. https://doi.org/10.1002/crat.200800149.

[30] S.M. Hossini Asl, M. Masomi, M. Tajbakhsh, Hybrid adaptive neuro-fuzzy inference systems for forecasting benzene, toluene & m-xylene removal from aqueous solutions by HZSM-5 nano-zeolite synthesized from coal fly ash, J. Clean. Prod. 258 (2020) 120688. https://doi.org/10.1016/j.jclepro.2020.120688.

[31] Y. Wang, Y. Chang, M. Liu, A. Zhang, X. Guo, A facile strategy to prepare shaped

ZSM-5 catalysts with enhanced para-xylene selectivity and stability for toluene methylation: The effect of in situ modification by attapulgite, Molecules. 24 (2019). https://doi.org/10.3390/molecules24193462.

[32] I. Hita, T. Cordero-Lanzac, F.J. García-Mateos, M.J. Azkoiti, J. Rodríguez-Mirasol, T. Cordero, J. Bilbao, Enhanced production of phenolics and aromatics from raw bio-oil using HZSM-5 zeolite additives for PtPd/C and NiW/C catalysts, Appl. Catal. B Environ. 259 (2019). https://doi.org/10.1016/j.apcatb.2019.118112.

[33] M. Thommes, K. Kaneko, A. V. Neimark, J.P. Olivier, F. Rodriguez-Reinoso, J. Rouquerol, K.S.W. Sing, Physisorption of gases, with special reference to the evaluation of surface area and pore size distribution (IUPAC Technical Report), Pure Appl. Chem. 87 (2015) 1051–1069. https://doi.org/10.1515/pac-2014-1117.

[34] N. Ramírez Bocanegra, J. Rivera De la Rosa, C.J. Lucio Ortiz, P. Cubillas González, H.C. Greenwell, V.E. Badillo Almaráz, L. Sandoval Rangel, B. Alcántar-Vázquez, V. Rodríguez-González, D.A. De Haro Del Río, Catalytic conversion of 5-hydroxymethylfurfural (5-HMF) over Pd-Ru/FAU zeolite catalysts, Catal. Today. 360 (2021) 2–11. https://doi.org/10.1016/j.cattod.2019.11.032.

[35] L. Bu, M.R. Nimlos, D.J. Robichaud, S. Kim, Diffusion of aromatic hydrocarbons in hierarchical mesoporous H-ZSM-5 zeolite, Catal. Today. 312 (2018) 73–81. https://doi.org/10.1016/j.cattod.2018.02.012.

[36] M.M. Yung, A.K. Starace, M.B. Griffin, J.D. Wells, R.E. Patalano, K.R. Smith, J.A. Schaidle, Restoring ZSM-5 performance for catalytic fast pyrolysis of biomass: Effect of regeneration temperature, Catal. Today. 323 (2019) 76–85. https://doi.org/10.1016/j.cattod.2018.06.025.

[37] R.E. Guedes, A.S. Luna, A.R. Torres, Operating parameters for bio-oil production in biomass pyrolysis: A review, J. Anal. Appl. Pyrolysis. 129 (2018) 134–149. https://doi.org/10.1016/j.jaap.2017.11.019.

[38] H. Aldana, F.J. Lozano, J. Acevedo, A. Mendoza, Thermogravimetric characterization and gasification of pecan nut shells, Bioresour. Technol. 198 (2015) 634–641. https://doi.org/10.1016/j.biortech.2015.09.069.

[39] X. Huang, J.P. Cao, X.Y. Zhao, J.X. Wang, X. Fan, Y.P. Zhao, X.Y. Wei, Pyrolysis kinetics of soybean straw using thermogravimetric analysis, Fuel. 169 (2016) 93–98. https://doi.org/10.1016/j.fuel.2015.12.011.

[40] S.A. El-Sayed, M.E. Mostafa, Pyrolysis characteristics and kinetic parameters determination of biomass fuel powders by differential thermal gravimetric analysis

(TGA/DTG), Energy Convers. Manag. 85 (2014) 165–172. https://doi.org/10.1016/j.enconman.2014.05.068.

[41] N. Johar, I. Ahmad, A. Dufresne, Extraction, preparation and characterization of cellulose fibres and nanocrystals from rice husk, Ind. Crops Prod. 37 (2012) 93–99. https://doi.org/10.1016/j.indcrop.2011.12.016.

[42] H.E. Kissinger, Reaction Kinetics in Differential Thermal Analysis, Anal. Chem. 29 (1957) 1702–1706. https://doi.org/10.1021/ac60131a045.

[43] A.K. Burnham, X. Zhou, L.J. Broadbelt, Critical review of the global chemical kinetics of cellulose thermal decomposition, Energy and Fuels. 29 (2015) 2906–2918. https://doi.org/10.1021/acs.energyfuels.5b00350.

[44] Y. Wang, Y. Liu, Z. Yu, Q. Yang, R. Ruan, B. Zhang, Z. Ma, D. Jiang, L. Dai, Q. Wu, S. Yang, L. Jiang, Co-pyrolysis of biomass and soapstock in a downdraft reactor using a novel ZSM-5/SiC composite catalyst, Bioresour. Technol. 279 (2019) 202–208. https://doi.org/10.1016/j.biortech.2019.01.119.

[45] B. Valle, A. Remiro, N. García-Gómez, A.G. Gayubo, J. Bilbao, Recent research progress on bio-oil conversion into bio-fuels and raw chemicals: a review, J. Chem. Technol. Biotechnol. 94 (2019) 670–689. https://doi.org/10.1002/JCTB.5758.

[46] F.X. Collard, J. Blin, A review on pyrolysis of biomass constituents: Mechanisms and composition of the products obtained from the conversion of cellulose, hemicelluloses and lignin, Renew. Sustain. Energy Rev. 38 (2014) 594–608. https://doi.org/10.1016/j.rser.2014.06.013.

[47] H. Zhang, S. Shao, R. Xiao, D. Shen, J. Zeng, Characterization of coke deposition in the catalytic fast pyrolysis of biomass derivates, Energy and Fuels. 28 (2014) 52–57. https://doi.org/10.1021/ef401458y.

[48] S. Wang, G. Dai, H. Yang, Z. Luo, Lignocellulosic biomass pyrolysis mechanism: A state-of-the-art review, Prog. Energy Combust. Sci. 62 (2017) 33–86.

[49] M. Ibáñez, B. Valle, J. Bilbao, A.G. Gayubo, P. Castaño, Effect of operating conditions on the coke nature and HZSM-5 catalysts deactivation in the transformation of crude bio-oil into hydrocarbons, Catal. Today. 195 (2012) 106–113. https://doi.org/10.1016/j.cattod.2012.04.030.

[50] D.G. Henry, I. Jarvis, G. Gillmore, M. Stephenson, Raman spectroscopy as a tool to determine the thermal maturity of organic matter: Application to sedimentary, metamorphic and structural geology, Earth-Science Rev. 198 (2019) 102936. https://doi.org/10.1016/J.EARSCIREV.2019.102936.

[51] B. Li, X. Xie, L. Zhang, D. Lin, S. Wang, S. Wang, H. Xu, J. Wang, Y. Huang, S. Zhang, D. Liu, Coke formation during rapid quenching of volatile vapors from fast pyrolysis of cellulose, Fuel. 306 (2021) 121658. https://doi.org/10.1016/J.FUEL.2021.121658.

[52] M. Ibáñez, M. Artetxe, G. Lopez, G. Elordi, J. Bilbao, M. Olazar, P. Castaño, Identification of the coke deposited on an HZSM-5 zeolite catalyst during the sequenced pyrolysis-cracking of HDPE, Appl. Catal. B Environ. 148–149 (2014) 436–445. https://doi.org/10.1016/j.apcatb.2013.11.023.

[53] P.S. Rezaei, H. Shafaghat, W.M.A.W. Daud, Production of green aromatics and olefins by catalytic cracking of oxygenate compounds derived from biomass pyrolysis: A review, Appl. Catal. A Gen. 469 (2014) 490–511. https://doi.org/10.1016/j.apcata.2013.09.036.

[54] R. Ruiz-Rosas, J. Bedia, M. Lallave, I.G. Loscertales, A. Barrero, J. Rodríguez-Mirasol, T. Cordero, The production of submicron diameter carbon fibers by the electrospinning of lignin, Carbon N. Y. 48 (2010) 696–705. https://doi.org/10.1016/j.carbon.2009.10.014.

[55] T. Cordero-Lanzac, R. Palos, J.M. Arandes, P. Castaño, J. Rodríguez-Mirasol, T. Cordero, J. Bilbao, Stability of an acid activated carbon based bifunctional catalyst for the raw bio-oil hydrodeoxygenation, Appl. Catal. B Environ. 203 (2017) 389–399. https://doi.org/10.1016/j.apcatb.2016.10.018.

[56] L.Y. Jia, M. Raad, S. Hamieh, J. Toufaily, T. Hamieh, M.M. Bettahar, G. Mauviel, M. Tarrighi, L. Pinard, A. Dufour, Catalytic fast pyrolysis of biomass: Superior selectivity of hierarchical zeolites to aromatics, Green Chem. 19 (2017) 5442–5459. https://doi.org/10.1039/c7gc02309j.

[57] Nishu, R. Liu, M.M. Rahman, M. Sarker, M. Chai, C. Li, J. Cai, A review on the catalytic pyrolysis of biomass for the bio-oil production with ZSM-5: Focus on structure, Fuel Process. Technol. 199 (2020) 106301. https://doi.org/10.1016/j.fuproc.2019.106301.

[58] A. Eschenbacher, P.A. Jensen, U.B. Henriksen, J. Ahrenfeldt, S. Ndoni, C. Li, J.Ø. Duus, U.V. Mentzel, A.D. Jensen, Catalytic deoxygenation of vapors obtained from ablative fast pyrolysis of wheat straw using mesoporous HZSM-5, Fuel Process. Technol. 194 (2019) 106119. https://doi.org/10.1016/j.fuproc.2019.106119.

[59] P. Fu, A. Zhang, S. Luo, W. Yi, S. Hu, Y. Zhang, Catalytic Steam Reforming of Biomass-Derived Acetic Acid over Two Supported Ni Catalysts for Hydrogen-Rich

Syngas Production, ACS Omega. 4 (2019) 13585–13593. https://doi.org/10.1021/acsomega.9b01985.

[60] P.D. Muley, C. Henkel, K.K. Abdollahi, C. Marculescu, D. Boldor, A critical comparison of pyrolysis of cellulose, lignin, and pine sawdust using an induction heating reactor, Energy Convers. Manag. 117 (2016) 273–280. https://doi.org/10.1016/j.enconman.2016.03.041.

[61] C. Ravikumar, P. Senthil Kumar, S.K. Subhashni, P.V. Tejaswini, V. Varshini, Microwave assisted fast pyrolysis of corn cob, corn stover, saw dust and rice straw: Experimental investigation on bio-oil yield and high heating values, Sustain. Mater. Technol. 11 (2016) 19–27. https://doi.org/10.1016/j.susmat.2016.12.003.

[62] D. Mohan, C.U. Pittman, P.H. Steele, Pyrolysis of wood/biomass for bio-oil: A critical review, Energy and Fuels. 20 (2006) 848–889. https://doi.org/10.1021/ef0502397.

[63] W. Tao, P. Zhang, X. Yang, H. Li, Y. Liu, B. Pan, An integrated study on the pyrolysis mecanism of peanut shell based on the kinetic analysis and solid/gas characterization, Bioresour. Technol. 329 (2021) 124860. https://doi.org/10.1016/J.BIORTECH.2021.124860.

[64] S. Wang, G. Dai, H. Yang, Z. Luo, Lignocellulosic biomass pyrolysis mechanism: A state-of-the-art review, Prog. Energy Combust. Sci. 62 (2017) 33–86. https://doi.org/10.1016/j.pecs.2017.05.004.

[65] S.S. Kim, F.A. Agblevor, Thermogravimetric analysis and fast pyrolysis of Milkweed, Bioresour. Technol. 169 (2014) 367–373. https://doi.org/10.1016/J.BIORTECH.2014.06.079.

[66] H.V. Ly, S.S. Kim, J.H. Choi, H.C. Woo, J. Kim, Fast pyrolysis of Saccharina japonica alga in a fixed-bed reactor for bio-oil production, Energy Convers. Manag. 122 (2016) 526–534. https://doi.org/10.1016/j.enconman.2016.06.019.

[67] C. Zhao, E. Jiang, A. Chen, Volatile production from pyrolysis of cellulose, hemicellulose and lignin, J. Energy Inst. (2016). https://doi.org/10.1016/j.joei.2016.08.004.

[68] G. Chang, Y. Huang, J. Xie, H. Yang, H. Liu, X. Yin, C. Wu, The lignin pyrolysis composition and pyrolysis products of palm kernel shell, wheat straw, and pine sawdust, Energy Convers. Manag. 124 (2016) 587–597. https://doi.org/10.1016/j.enconman.2016.07.038.

[69] S. Wang, B. Ru, H. Lin, W. Sun, Z. Luo, Pyrolysis behaviors of four lignin polymers isolated from the same pine wood, Bioresour. Technol. 182 (2015) 120–127.

https://doi.org/10.1016/J.BIORTECH.2015.01.127.

[70] A.A. Boateng, C.A. Mullen, N.M. Goldberg, K.B. Hicks, T.E. Devine, I.M. Lima, and J.E. McMurtrey, Sustainable production of bioenergy and biochar from the straw of high-biomass soybean lines via fast pyrolysis, Environ. Prog. Sustain. Energy. 29 (2010) 175–183. https://doi.org/10.1002/ep.10446.

[71] L. Dunnigan, P.J. Ashman, X. Zhang, C.W. Kwong, Production of biochar from rice husk: Particulate emissions from the combustion of raw pyrolysis volatiles, J. Clean. Prod. 172 (2018) 1639–1645. https://doi.org/10.1016/j.jclepro.2016.11.107.

[72] G. Offen, R. Himes, S. Tavoulareas, Volatile Products of Oxidative Pyrolisis of Wood: Influence of Ions, J. Anal. Appl. Pyrolysis. 17 (1990) 261–273. https://doi.org/10.1016/0165-2370(90)85015-F.

[73] J.M. Rosas, J. Bedia, J. Rodríguez-Mirasol, T. Cordero, On the preparation and characterization of chars and activated carbons from orange skin, Fuel Process. Technol. 91 (2010) 1345–1354. https://doi.org/10.1016/J.FUPROC.2010.05.006.

[74] D. Lozano-Castelló, D. Cazorla-Amorós, A. Linares-Solano, Usefulness of CO2 adsorption at 273 K for the characterization of porous carbons, Carbon N. Y. 42 (2004) 1233–1242. https://doi.org/10.1016/J.CARBON.2004.01.037.

[75] D. Cazorla-Amorós, J. Alcañ Iz-Monge, M.A. De La Casa-Lillo, A. Linares-Solano, CO 2 As an Adsorptive To Characterize Carbon Molecular Sieves and Activated Carbons, (1998). https://pubs.acs.org/sharingguidelines (accessed November 25, 2021).

[76] J. Pallarés, A. González-Cencerrado, I. Arauzo, Production and characterization of activated carbon from barley straw by physical activation with carbon dioxide and steam, Biomass and Bioenergy. 115 (2018) 64–73. https://doi.org/10.1016/j.biombioe.2018.04.015.

[77] J. Rodriguez-Mirasol, T. Cordero, J.J. Rodriguez, Activated carbons from carbon dioxide partial gasification of eucalyptus kraft lignin, Energy and Fuels. 7 (2002) 133–138. https://doi.org/10.1021/EF00037A021.

[78] J.G.D. Tadimeti, R. Thilakaratne, V.K. Balla, K.H. Kate, J. Satyavolu, A two-stage C5 selective hydrolysis on soybean hulls for xylose separation and value-added cellulose applications, Biomass Convers. Biorefinery. (2020) 1–13. https://doi.org/10.1007/S13399-020-00860-5/FIGURES/7.

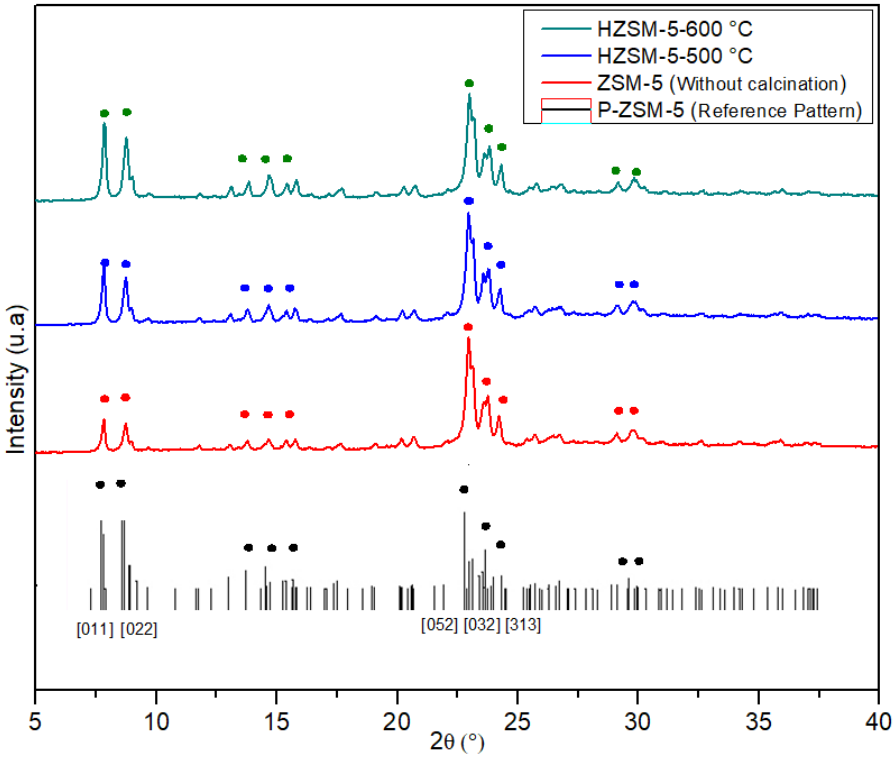

Fig. 1. XRD of the HZSM-5 zeolite at different calcination temperatures

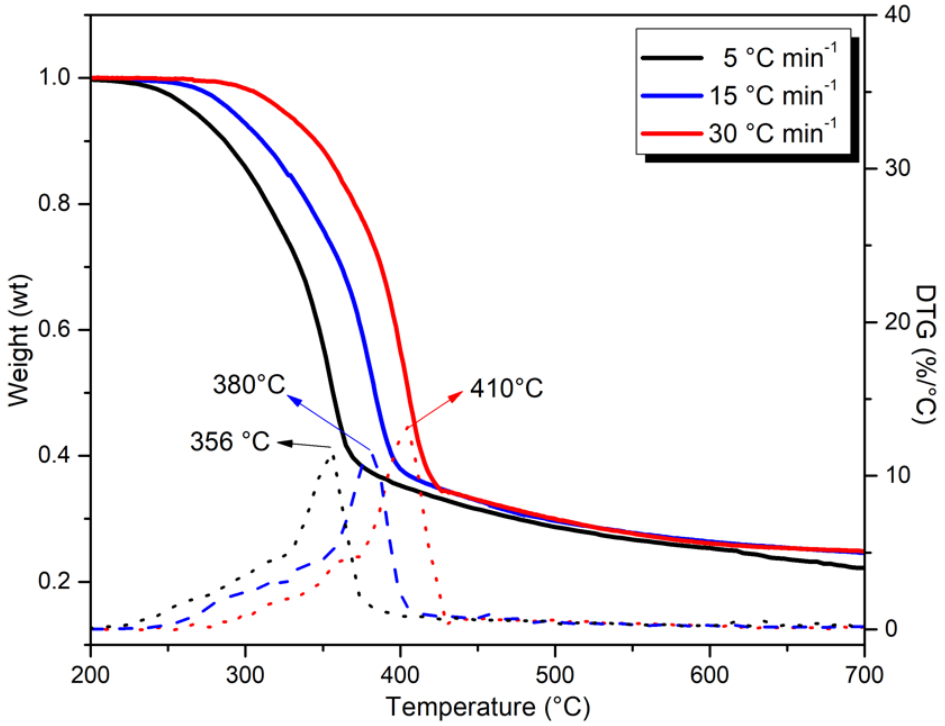

Fig. 2. TG (solid lines) and DTG (dotted lines) profiles of SH at different heating rates of 5, 10, 30 °C min^{-1}

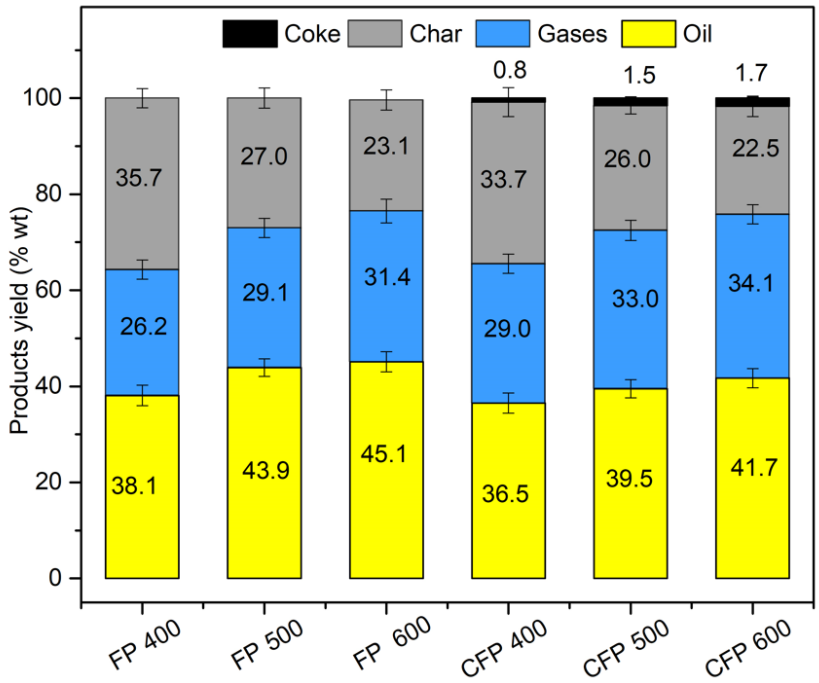

Fig. 3. Product distribution from FP and CFP experiments of the SH at different pyrolysis temperatures

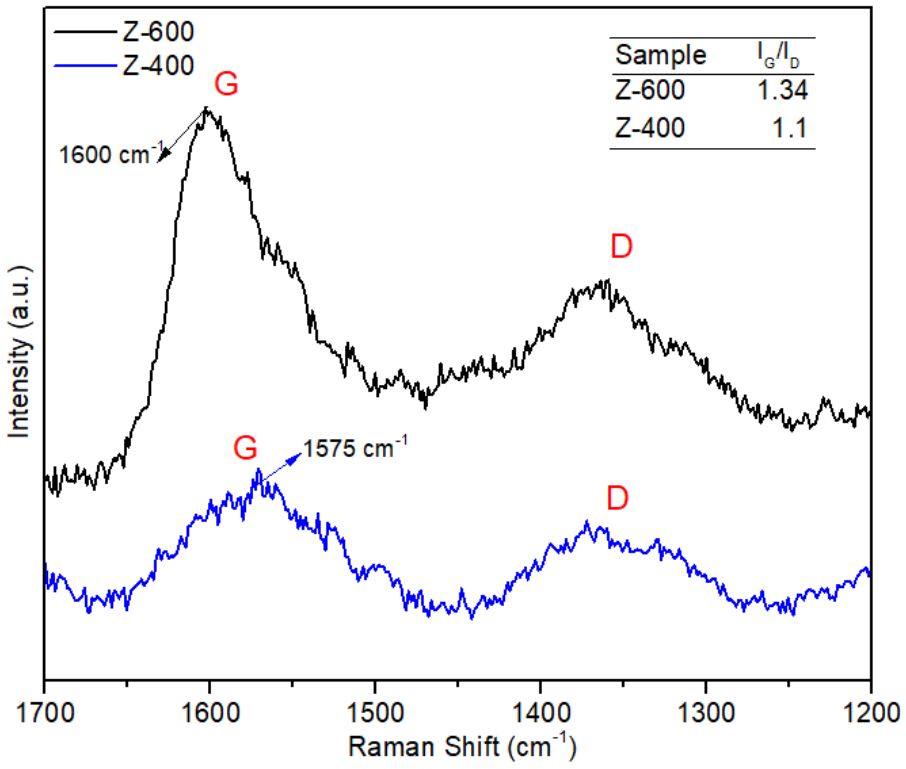

Fig. 4. Raman spectra of the coke deposited on the HZSM-5 zeolite used at 400 °C (Z-400) and 600 °C (Z-600)

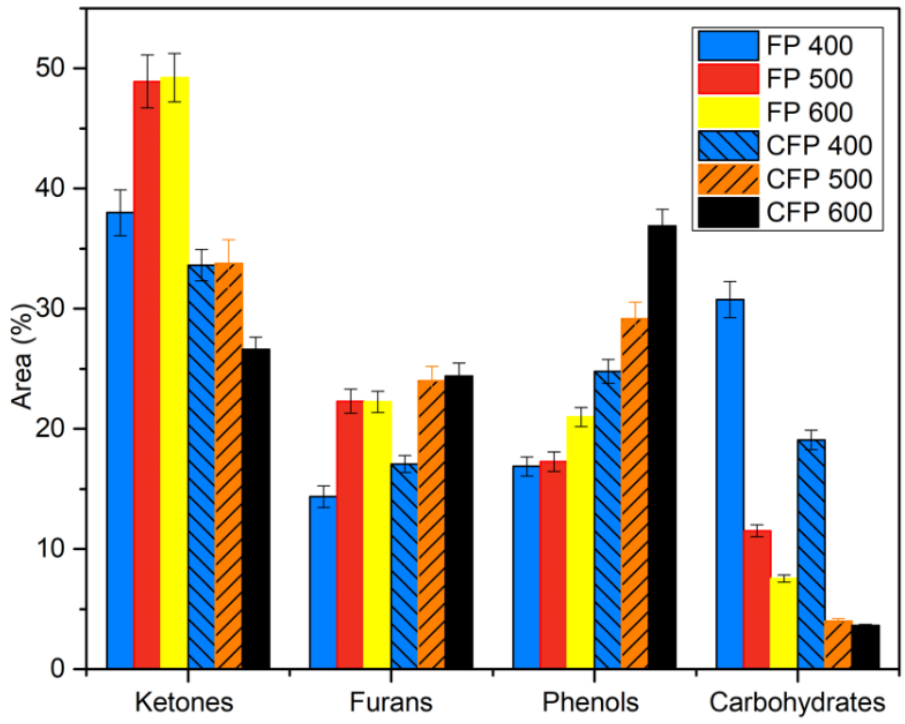

Fig. 5. GC-MS derived distribution of chemical compounds in the bio-oil obtained by FP and CFP at different temperatures

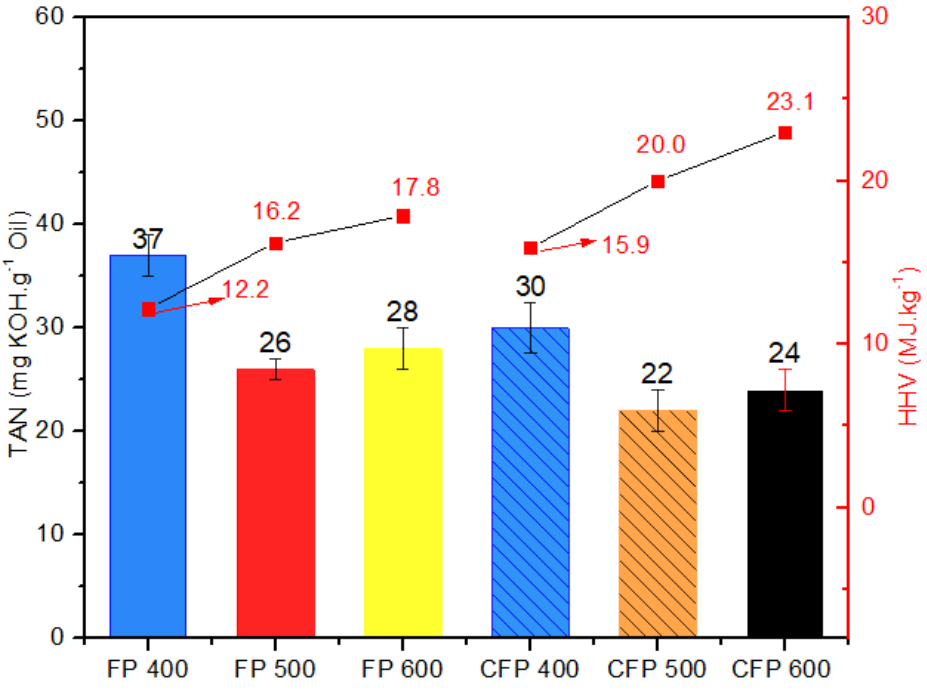

Fig. 6. Total acid number (TAN) and the higher heating value (HHV) of the FP and CFP of SH.

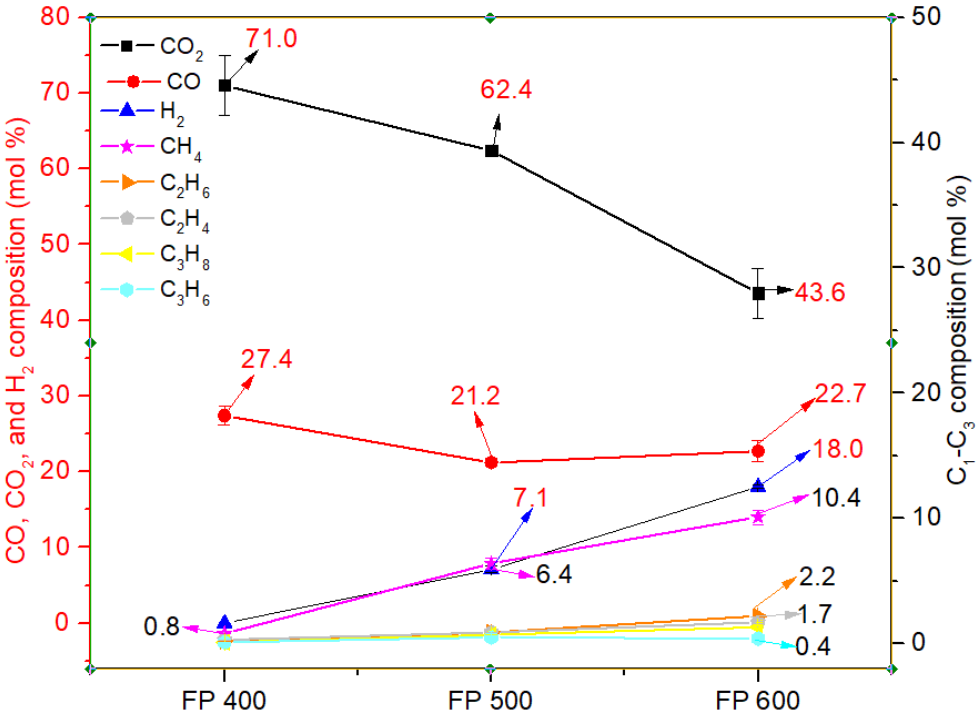

Fig. 7. Molar Composition of the gases of the FP of SH

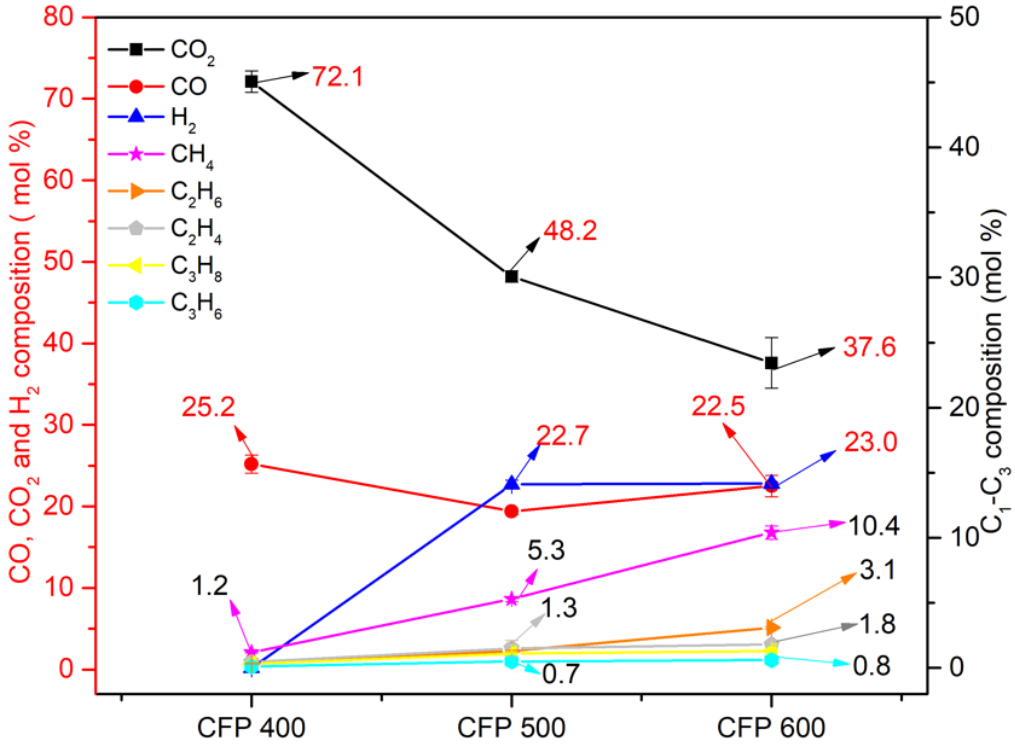

Fig. 8. Molar composition of the gases of the CFP of SH

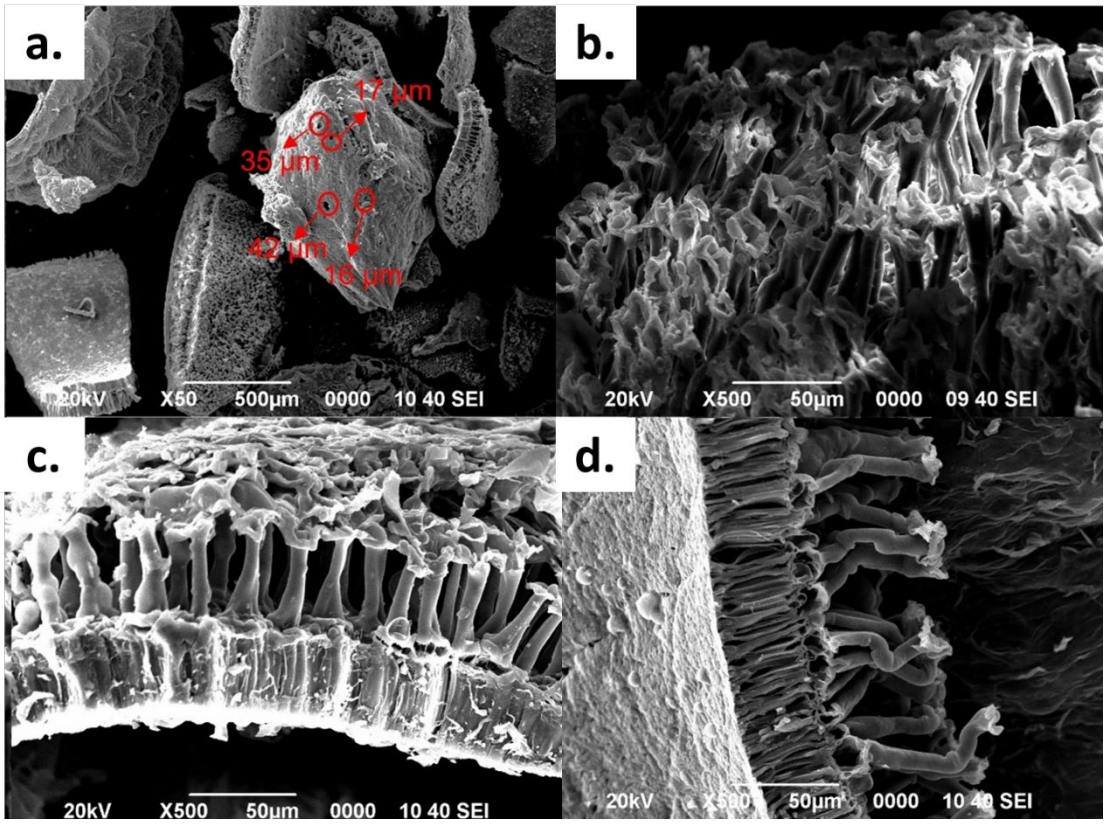

Fig. 9. Scanning electron micrographs of the char obtained from pyrolysis of SH at a) lower magnification of char obtained at 500 ºC, b) 400 °C, c) 500 °C and d) 600 °C.

Table 1. Main compounds and composition (%) as determined by GC-MS obtained from the FP and CFP of SH

Classification	Compound	Type of pyrolysis-Temperature (°C)					
		FP400	FP500	FP600	CFP400	CFP500	CFP600
Ketones	Cyclopentanone	0.5	0.8	1.9	1.4	0.6	2.7
	2-Cyclopenten-1-one	6.1	4.2	5.5	1.6	7.9	2.1
	2-Cyclopenten-1-one, 2-Methyl-	2.6	3.4	5.1	3.7	0.0	4.5
	1,2-Cyclooctanedione	0.9	1.1	0.5	1.5	0.0	0.6
	2-cyclopenten-1-one, 3-Methyl-	1.2	4.3	9.0	0.3	3.5	4.2
	1,2-Cyclooctanedione	0.0	1.1	0.5	1.5	0.0	0.6
	2-Cyclopenten-1-one, 2-hidroxy-3-methyl	3.3	9.3	14.2	1.7	13.6	3.0
	1,2-Cyclopentadione, 3-methyl-	3.4	5.5	9.0	3.5	0.0	2.1
	1,2-Cyclopentadione, 3-methyl-	0.0	7.8	0.0	3.5	0.0	0.0
	2-Cyclopenten-1-one, 2-hydroxy-3,4 dimethyl	11.0	4.1	2.1	6.4	0.0	1.6
	2-Cyclopenten-1-one, 3-Ethyl-2-hydroxy	9.1	7.4	2.5	8.5	8.2	5.3
Furans	2-Furaldehyde (Furfural)	0.0	0.7	1.4	1.0	1.7	0.9
	2-Furanmethanol (Furfuryl alcohol)	11.3	8.1	9.5	3.5	5.1	5.3
	2-Acetylfuran	1.6	2.6	1.4	2.2	0.0	0.5
	2(5H)-Furanone	1.4	6.9	4.9	4.8	4.2	5.2
	2(5H)-Furanone, 5-methyl-	0.0	0.9	0.9	0.9	0.0	1.4
	5-Methylfurfural	0.0	2.9	3.2	0.7	1.1	1.6
	Other furans	0.0	0.0	0.0	4.1	11.8	9.4
Phenol	Phenol	2.6	1.4	3.3	0.7	5.2	9.4
	Phenol, 2-methyl (o-cresol)	9.3	6.2	8.2	10.5	5.3	2.8
	Phenol, 3-methyl- (p-cresol)	3.7	6.7	5.6	3.4	5.8	7.2
	Phenol, 4-methyl- (m-cresol)	1.3	3.0	3.8	4.8	4.2	9.6
	Other phenols	0.0	0.0	0.0	5.3	8.6	3.9
Carbohydrates	1,4,3,6-Dianhydro-D-glucopyranoce	19.6	10.5	4.5	9.5	3.1	1.3
	Levoglucosan	11.1	1.0	3.1	9.6	0.9	2.2

Table 2. Main compounds and composition (%) as determined by GC-MS CFP

Classification	Compound	Type of pyrolysis-Temperature (°C)		
		CFP-400	CFP-500	CFP-600
Furans	Furfural	0.2	0.6	0.2
	Furan, 2-methyl-	0.5	3.5	1.3
	Furan, 3-methyl-	1.6	3.6	2.4
	Furan, 2-ethyl	1.7	2.3	5.2
	5-Methylfurfural	0.1	1.1	1.5
Hydrocarbons	Ethylbenzene	0.4	1.5	0.6
	p-Xylene	2.7	1.5	4.2
	1,3,5,6,7-Cyclooctatetraene	0.6	2.1	0.6
	1-Methylcyclopentene	1.6	2.0	2.0
	Cyclohexene	0.4	1.4	0.7
Phenols	Phenol, 3,5-dimethyl	1.3	2.4	2.6
	Phenol, 2,5-dimethyl	3.0	4.8	3.4
	Phenol, 2-ethyl-6methyl-	1.1	0.9	6.9

Table 3. Mass yield and HHV of gases in the FP and CFP of the SH at different temperatures.

Pyrolysis	CO	CO_2	H_2	CH_4	C_2H_6	C_2H_4	C_3H_8	C_3H_6	HHV
	Mass yield, % wt								(kJ/m^3)
FP 400	3.81±0.17	15.34±0.84	*	*	*	*	*	*	4.4
FP 500	4.92±0.11	18.91±0.20	0.11±0.01	0.78±0.05	0.20±0.01	0.18±0.01	0.22±0.01	0.16±0.01	9.2
FP 600	6.09±0.45	19.65±0.16	3.61±0.01	1.62±0.11	0.65±0.03	0.47±0.02	0.57±0.04	0.18±0.01	14.8
CFP 400	3.99±0.18	18.00±0.32	*	1.10±0.10	0.60±0.02	0.70±0.03	0.80±0.03	*	4.9
CFP 500	5.27±0.13	20.53±0.30	0.44±0.01	0.82±0.03	0.36±0.01	0.42±0.02	0.45±0.03	0.20±0.01	11.2
CFP 600	8.04±0.47	21.09±0.71	0.58±0.03	2.13±0.11	1.18±0.02	0.63±0.05	0.71±0.04	0.28±0.01	15.6

*Value < 0.1 % g·g^{-1}

Table 4. Elemental, proximal and inorganic material analysis of char obtained at different temperatures

	Temperature (°C)		
Sample	**400**	**500**	**600**
Ultimate analysis (wt. **%**)			
C	67.9	70.5	74.4
H	3.8	3.1	2.4
O	14.2	12	7.6
N	2.2	1.9	1.6
Calorific value (MJ kg^{-1})			
HHV	25.9	26.2	27.2
Proximate analysis (wt. **%**)			
V.M.	45	39	36
[b]F.C	43	47	48
Ash	12	13	15
Inorganic elements (wt. **%**)			
K_2O	6.1	6.1	7.4
CaO	3.9	4.1	4.8
MgO	0.6	0.7	0.7
Fe_2O_3	0.4	0.4	0.5
P_2O_5	0.3	0.4	0.5
BaO	0.2	0.2	0.3

VM: volatile matter; FC: fixed carbon. b Calculated by difference.

Table 5. Textural parameters of chares obtained at different temperatures

Temperature (ºC)	$S_{BET}^{N_2}$ cm^3g^{-1}	$V_T^{N_2}$ cm^3g^{-1}	$S_{DR}^{CO_2}$ m^2g^{-1}	$V_{DR}^{CO_2}$ cm^3g^{-1}
400	1.2	0.002	143	0.06
500	5.7	0.003	190	0.08
600	7.2	0.004	259	0.10

Supplementary material

CATALYTIC FAST PYROLYSIS OF SOYBEAN HULLS: FOCUS ON THE PRODUCTS

Jose Luis Toro-Trochez[a,b], David Alejandro De Haro Del Río[a], Ladislao Sandoval-Rangel[c], Diana Bustos-Martínez[a], Francisco José García-Mateos[b], Ramiro Ruiz-Rosas[b], José Rodríguez-Mirasol[b], Tomás Cordero[b], Eileen Susana Carrilo-Pedraza[a,*]

[a] Universidad Autónoma de Nuevo León, Facultad de Ciencias Químicas, Ave. Universidad S/N, Cd. Universitaria, San Nicolás de los Garza, N.L., C.P. 66455, *México.*

[b]Universidad de Málaga, Andalucía Tech, Departamento de Ingeniería Química, 29010 Málaga, Spain.

[c] Tecnológico de Monterrey, Escuela de Ingeniería y Ciencias, Ave. Eugenio Garza Sada 2501, Monterrey, N.L., 64849, México.

(*) E-mail: eileen.carrillopd@uanl.edu.mx

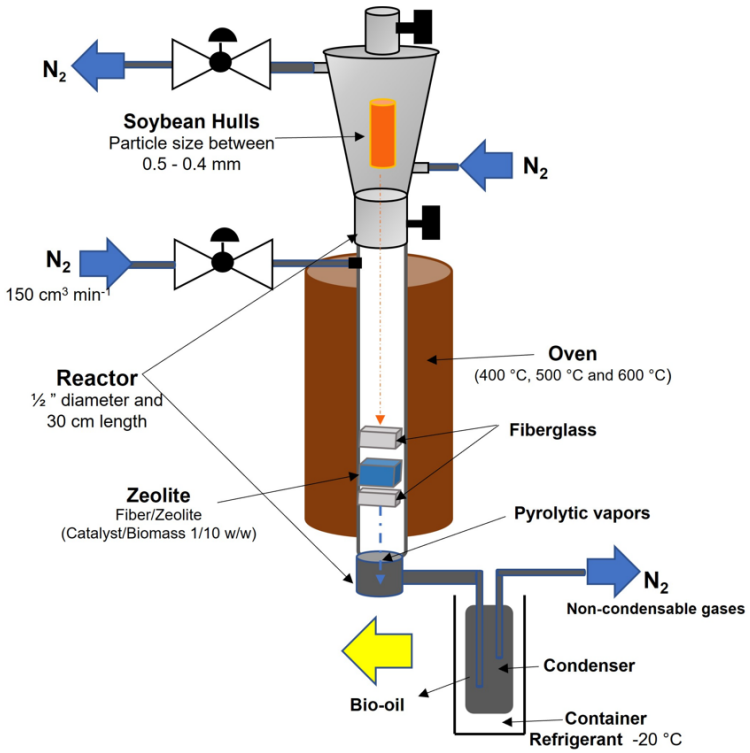

Fig. S1. Diagram scheme Catalytic Fast pyrolysis.

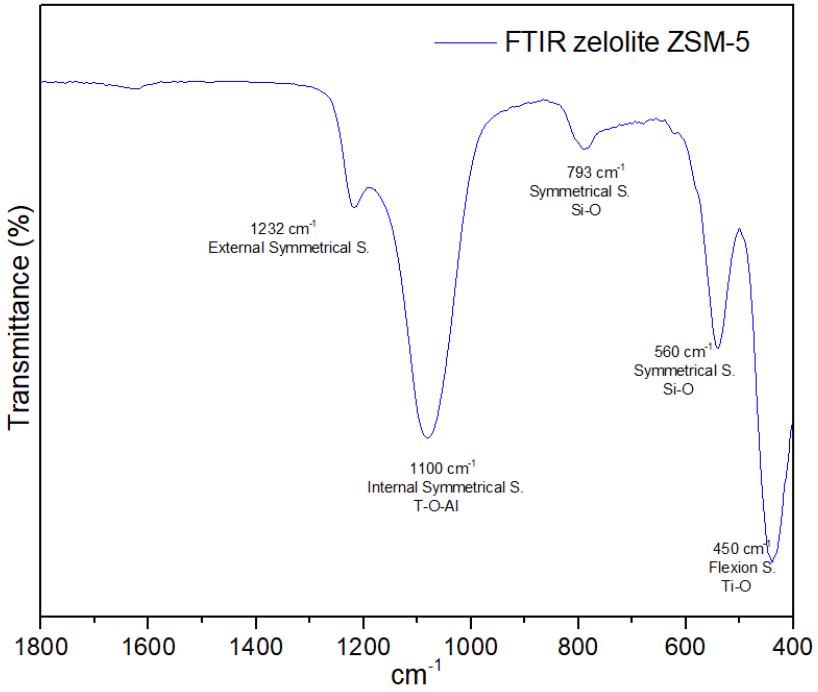

Fig. S2. FTIR of HZSM-5 zeolite

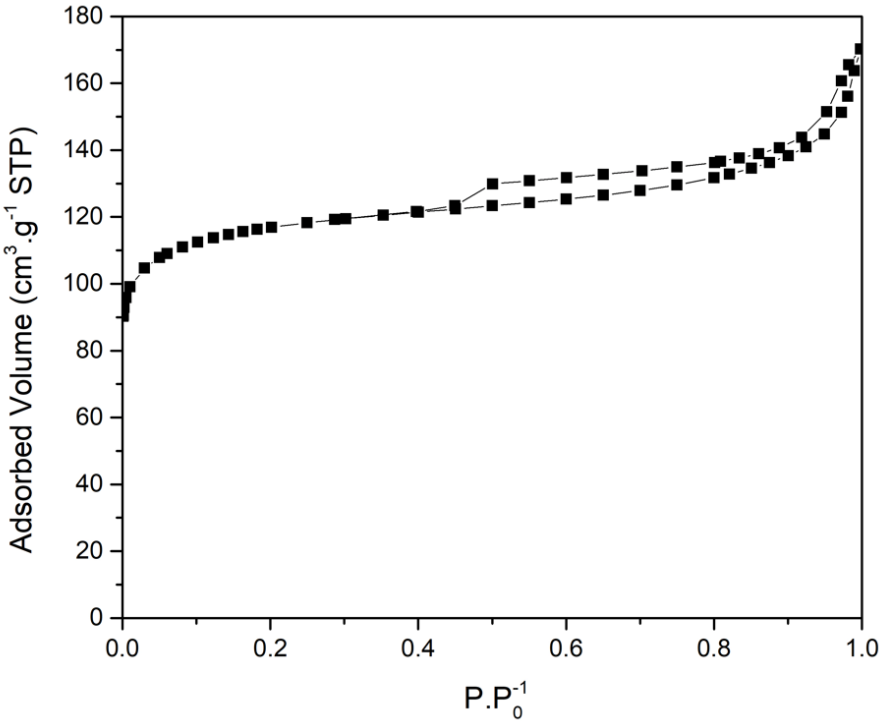

Fig. S3. HZSM-5 zeolite N_2 adsorption-desorption isotherm at -196 ºC

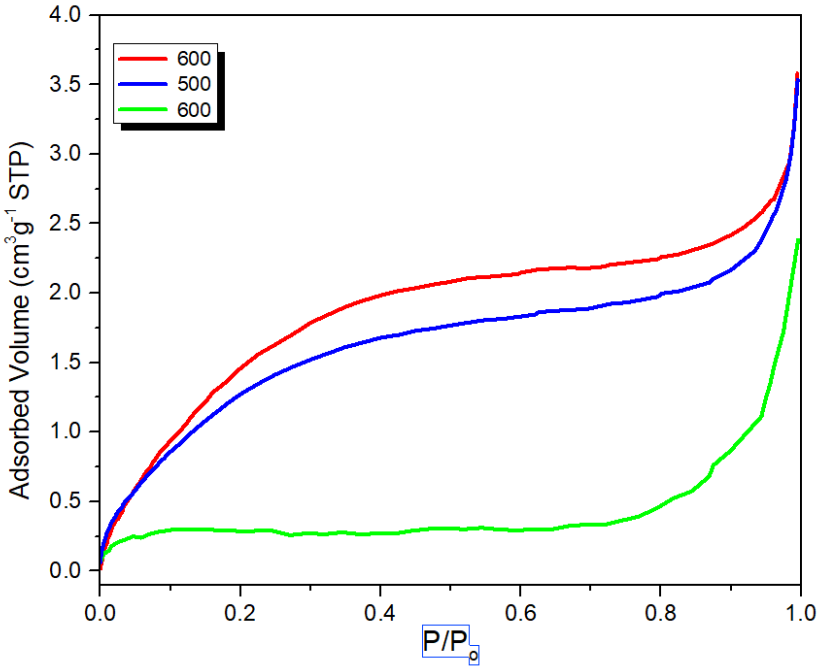

Fig. S4. N_2 Adsorption isotherm at -196 ºC of char obtained at different pyrolysis temperatures

Table S1. Textural properties of the HZSM-5 zeolite

Sample	S_{Total}[a] m^2g^{-1}	V_T[b] cm^3g^{-1}	V_{mic}[c] cm^3g^{-1}	s_{mi}[d] m^2g^{-1}	V_{meso}[e] cm^3g^{-1}
HZSM-5	450	0.22	0.16	415	0.06
Z-600	232	0.17	0.08	198	0.04

[a] BET surface area. [c] Total Volume pore obtained the N_2 isotherm. [c] Micropore volume obtained from the t-plot. [e] Mesopore volume calculated as $V_{meso} = V_T\ (P/P_0 = 0.95) - V_{mic}$

Table S2. Molar concentration of non-condensable gases of FP and CFP at different temperatures.

Pyrolysis	CO	CO_2	H_2	CH_4	C_2H_6	C_2H_4	C_3H_8	C_3H_6	HHV (kJ/molN)
	(mol%)								
FP 400	27.4±1.2	71.0±3.9	0.0±0.0	0.80±0.03	0.21±0.01	0.29±0.01	0.14±0.01	0.11±0.01	4.4
FP 500	21.2±0.6	62.4±1.0	7.1±0.4	6.4±0.4	0.9±0.02	0.9±0.02	0.7±0.03	0.5±0.01	9.2
FP 600	22.7±1.4	43.6±3.2	18.0±0.2	10.1±0.6	2.2±0.07	1.7±0.07	1.3±0.08	0.4±0.02	14.8
CFP 400	25.2±1.1	72.1+1.3	0.17±0.01	1.2±0.1	0.34±0.01	0.46±0.02	0.31±0.02	0.10±0.01	4.9
CFP 500	19.4±0.4	48.2±0.7	22.7±0.5	5.4±0.2	1.3±0.06	1.5±0.06	1.1±0.06	0.5±0.06	11.2
CFP 600	22.5±1.3	37.6±3.1	23.0±0.2	10.4±0.5	3.1±0.1	1.8±0.1	1.3±0.07	0.6±0.05	15.6